Available online at www.sciencedirect.com
SCIENCE DIRECT
Journal of Power Sources 153 (2006) 251–257
JOURNAL OF POWER SOURCES
www.elsevier.com/locate/jpowsour

A kinetics study of self-discharge of spinel electrodes in $Li/Li_xMn_2O_4$ cells

R. Yazami *, Y. Ozawa

The CNRS-CALTECH International Laboratory on Materials for Electrochemical Energetics, California Institute of Technology, MC 138-78, Pasadena, CA 91125, USA

Available online 14 November 2005

Abstract

The rate of self-discharge in lithium half-cells with the spinel-type $LiMn_2O_4$ cathode was investigated in the 60–75 °C temperature range. The time dependence of the capacity loss and the open-circuit voltage (OCV) was monitored during the thermal aging. Lithium re-intercalation from the electrolyte appears to govern the mechanism of self-discharge in the two plateaus at the '4 V' areas. Treatment of the OCV data acquired during aging and by the Galvanostatic Intermittent Titration Technique (GITT) method allowed the electrode composition to be determined during the course of self-discharge. Self-discharge current was then determined and plotted against OCV. The isothermal voltammograms obtained show characteristic self-discharge current peaks.

Keywords: Self-discharge; Capacity loss; Kinetics; Lithium manganese spinel; Activation energy

1. Introduction

Self-discharge occurs naturally in primary and secondary batteries and results in a decrease in the available capacity with storage time [1]. The rate of capacity loss depends mainly on the cell's chemistry, its state of charge and temperature. Other factors such as the specific surface area of the active electrodes materials, the storage environment (i.e. humidity), the cell engineering and purity of active (electrodes, electrolyte) and inactive (electron conductors, substrate, connectors, separator, . . .) materials may play a role. The main driving force of self-discharge in advanced technology batteries is due to the electric potential of one or both electrodes falling outside the thermodynamic stability window of the electrolyte. The electrolyte may then oxidize at the positive electrode (cathode) or reduce at the negative electrode (anode). The amounts of electricity used in these internal reactions are thus no longer available for the subsequent battery discharge. Eventually self-discharge involves a decrease in the open-circuit voltage (OCV) with the storage time. This is particularly true in lithium ion batteries, whose chemistry is based on Li intercalation-type reactions.

Typical lithium ion batteries use mainly graphite for the anode and a lithiated transition metal oxide for the cathode. Lithium cobalt oxide ($LiCoO_2$) is the most commonly used for this application [2]. However, the high cost of Co together with its limited availability and toxicity have become serious matters of concern, considering the rapidly growing market demand for high energy density secondary batteries. Over the last decade, a tremendous amount of research has been devoted to developing alternative cathodes to $LiCoO_2$. Among important candidates, the spinel-type $LiMn_2O_4$ has generated the highest R&D activity as Mn is cheaper, more abundant and environmentally more benign than Co [3–5]. Co- and Mn-based lithium ion batteries yield equivalent energy storage capabilities at ambient temperatures. Where $LiMn_2O_4$ discharges at higher voltage and sustains higher charge and discharge rates, $LiCoO_2$ has higher specific capacity ($mAh\,g^{-1}$) and energy density ($Wh\,kg^{-1}$). However, the energy cost ($\$\,Wh^{-1}$) should in principle be lower in $LiMn_2O_4$ [6].

Despite attractive characteristics, $LiMn_2O_4$ suffers from premature capacity loss upon cycling and/or aging at temperatures above 50 °C [7–27]. This was attributed to different factors including: (i) the Mn electrolyte dissolution [9–15,17,18,20,22,26,28–30], (ii) the instability in the two-phase system of the '4 V' area [9,15,23,31], (iii) the thermodynamically or kinetically induced cubic to tetragonal phase ($Li_2Mn_2O_4$) transition involving the Jahn–Teller lattice

* Corresponding author. Tel.: +1 6263954496; fax: +1 6267956132.
E-mail addresses: yazami@caltech.edu (R. Yazami), ozawa@caltech.edu (Y. Ozawa).

0378-7753/$ – see front matter © 2005 Elsevier B.V. All rights reserved.
doi:10.1016/j.jpowsour.2005.10.012

distortion [12,13,19,31–34], (iv) the formation of a passivation layer on the grains surface [18,20,23,35] and (v) the electrolyte decomposition [7–9,23].

Several quantitative studies on the capacity loss in $LiMn_2O_4$ have appeared in the literature [7,8,10,13,15,16,23,26,27]; however, none specifically studied the determination of instantaneous rates of self-discharge, especially during aging at high temperatures. In this work, we used experimental half-cells with a metallic lithium anode and manganese spinel cathode to investigate the kinetics of self-discharge due to the cathode. Based on the OCV versus composition and time measurements at different temperatures, we developed a method to assess the self-discharge current, which cannot be measured directly.

2. Theoretical considerations

A cell at its initial state of charge can deliver a discharge capacity $q(0)$. After it has been stored for a period of time t at temperature T, the cell's available capacity $q(t, T)$ will decline at a rate:

$$i(t, T) = -\frac{\partial q(t, T)}{\partial t}, \tag{1}$$

In Eq. (1), $i(t, T)$ is equivalent to a self-discharge current.

Assuming self-discharge in $LiMn_2O_4$ is governed by the lithium re-intercalation from the electrolyte [7–9] following the scheme:

$$Li_\varepsilon Mn_2O_4 + xLi^+ + xe^- \leftrightarrow Li_{\varepsilon+x}Mn_2O_4, \tag{2}$$

where $Li_\varepsilon Mn_2O_4$ denotes the delithiated spinel λ-MnO_2 which contains a small amount of Li, ε [36], the self-discharge current can be expressed as:

$$i(t, T) = -\frac{\partial q(t, T)}{\partial t} = n_0 F \frac{\partial x(t, T)}{\partial t}, \tag{3}$$

where n_0 is the initial number of $LiMn_2O_4$ (mole) and F is the Faraday number. To determine $i(t, T)$ requires the instantaneous electrode composition $x(t, T)$ to be known. The latter is obviously a difficult task as the available capacity cannot be directly accessible without discharging the cell. One way to indirectly access $x(t, T)$ is by comparing the OCV curves during thermal aging, $e(t, T)$ with the OCV versus composition curve, $e(x, T)$. The latter can be obtained by a titration technique such as the Galvanostatic Intermittent Titration Technique (GITT) [37]. In principle, the $e(t, T)$ curve can be compared to the $e(x)$, which, once equalized, leads to the $x(t, T)$ curve, provided the thermal coefficient $\left.\frac{\partial e(x,T)}{\partial T}\right|_x$ is known.

Eq. (3) can be developed as:

$$-\frac{\partial q(t, T)}{\partial t} = n_0 F \frac{\partial x(t, T)}{\partial t} = n_0 F \left.\frac{\partial x(t, T)}{\partial e}\right|_T \left.\frac{\partial e(t, T)}{\partial t}\right|_T = n_0 F \frac{\left.\frac{\partial e(t,T)}{\partial t}\right|_T}{\left.\frac{\partial e(x,T)}{\partial x}\right|_T} \tag{4}$$

In Eq. (4), $\left.\frac{\partial e(t,T)}{\partial t}\right|_T$ is the time slope of the chronopotentiometric isotherm $e(t, T)$, which can be directly monitored during aging. The $\left.\frac{\partial e(x,T)}{\partial x}\right|_T$ term is the slope of the $e(x, T)$ isotherm, which can be obtained by GITT, for example. A temperature correction should be made to account for the fact that $e(t, T)$ and $e(x, T)$ should be measured at the same temperature. If $e(x)$ is available only at ambient temperature T_0, one can determine it at a different temperature T by using the entropy function of lithium intercalation $\Delta S(x)$ and applying the following equation:

$$e(x, T) = e(x, T_0) + \frac{T - T_0}{F} \Delta S(x), \tag{5}$$

3. Experimental

Spinel-based cathodes were provided by courtesy of ENAX, Japan. Elemental analysis gives a composition close to $Li_{1.08}Mn_{1.92}O_4$, which will be designed hereafter $LiMn_2O_4$ for simplicity. The cathodes consisted of aluminum coated with a composite electrode having 89 wt.% $LiMn_2O_4$, 5 wt.% PVDF and 6 wt.% of fine graphite powder. Half-cells with coin-type design (CR 2016) of Li/$LiClO_4$ 1 M in PC/$LiMn_2O_4$ configuration were mounted into a dry box filled with argon. A glass fiber separator from Crane Co. (USA) (Craneglas 230/6.1) was used. The cells were cycled five times between 3.0 and 4.4 V under C/5 rate at an ambient temperature of $23 \pm 1\,^\circ C$, the last step being a charge to 4.4 V. The cells were then heated in a furnace with controlled temperatures (±0.5 °C) of 60, 65, 70 and 75 °C. The cells were aged for a period up to 42 days and the OCV ($e(t, T)$) was recorded. The cells were then cooled to ambient temperature and discharged to 3 V at C/5 rate. This was followed by a few cycles between 3 and 4.4 V. The OCV versus composition curve $e(x)$ was obtained at the ambient temperature using GITT. Starting from the fully charged state at 4.4 V, the composition was incremented galvanostatically by $\Delta x = 0.05$ after applying a C/20 rate current for 1 h. The cell was then rested until a stable OCV was reached, before performing the next composition increment.

4. Results and discussion

4.1. Capacity loss

A typical cycle capacity profile before and after aging for 6 days at 75 °C is shown in Fig. 1. The initial capacity during the first five cycles stabilized at around $Q_i \sim 120\,mAh\,g^{-1}$. The discharge capacity after aging fell to $Q_a \sim 20\,mAh\,g^{-1}$, which corresponds to a total capacity loss Q_{tcl} of around $100\,mAh\,g^{-1}$. The capacity recovered during the following cycles reached $\sim 80\,mAh\,g^{-1}$. Accordingly, the capacity loss has two terms; a recoverable (reversible) capacity loss $Q_{rcl} = 80 - 20 = 60\,mAh\,g^{-1}$ and an irrecoverable (irreversible) capacity loss $Q_{icl} = 120 - 80 = 40\,mAh\,g^{-1}$.

The time dependence of Q_{tcl}, Q_{rcl} and Q_{icl} at different storage temperatures is plotted in Fig. 2a–c, respectively. In addition to results on $LiMn_2O_4$, Fig. 2a includes those obtained with

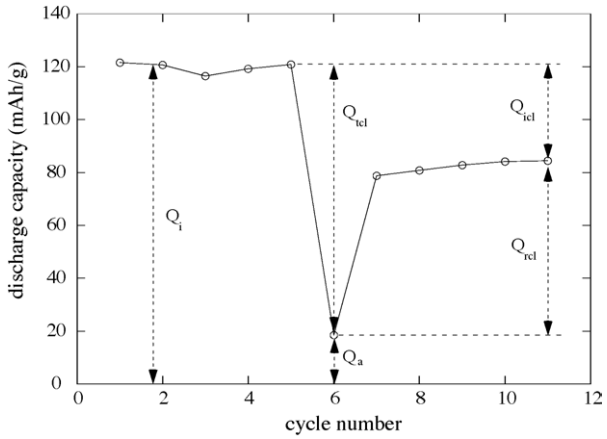

Fig. 1. Cycle capacity profile before and after aging at 75 °C for 6 days of a $Li/Li_xMn_2O_4$ half cell.

$LiCoO_2$ (noted LCO) at 60 and 75 °C, which are shown here for comparison.

The capacity loss data were fitted with the following empirical law:

$$t = A(T)y^2 + By, \tag{6}$$

in which y is the relative capacity loss given by:

$$y\frac{Q_{tc1}}{Q_i} \times 100, \tag{7}$$

In Eq. (6), the temperature dependant '$A(T)$' coefficient follows the Arrhenius law, with activation energy of $E_{acl} = 83.2\,kJ\,mole^{-1}$. The recoverable and irrecoverable capacity losses increased with temperature and their time dependences were fit quite well with $\sqrt{t}$ and linear time functions, respectively. As we reported earlier [38], Eq. (6) applied as well to the $LiCoO_2$ cathode and a corresponding activation energy of $81.2\,kJ\,mole^{-1}$ was found. Note the proximity of the activation energy values obtained from the capacity loss data in $LiMn_2O_4$ and $LiCoO_2$. However, in comparing the two cathode

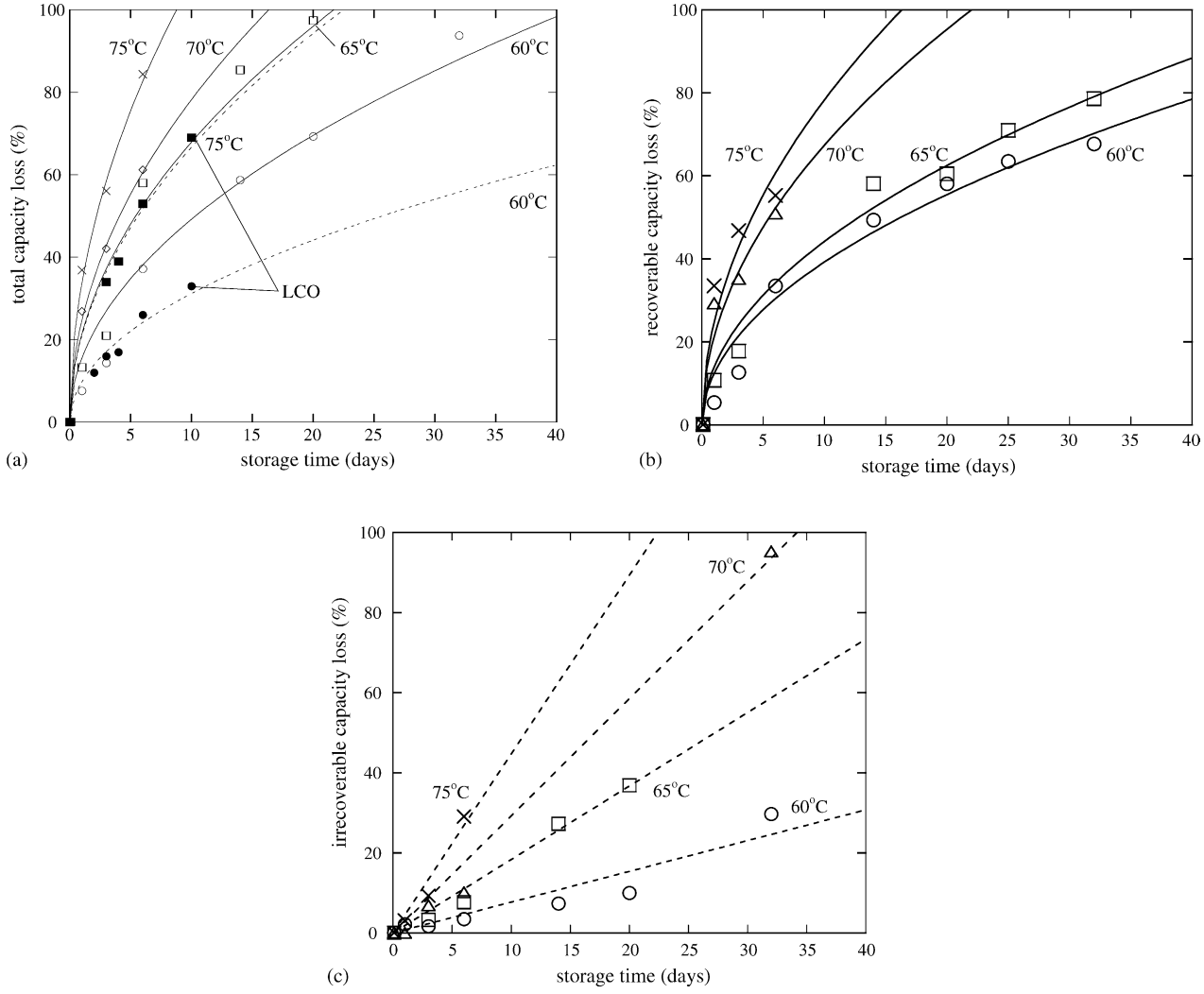

Fig. 2. Time dependence of the total (a), recoverable (b) and irrecoverable (c) capacity losses at different aging temperature. (a) Results on the $LiCoO_2$ cathode at 60 and 75 °C for comparison.

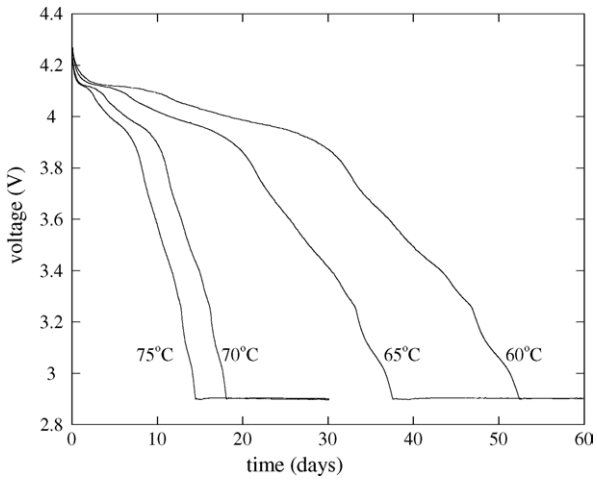

Fig. 3. The OCV vs. time curves profiles during aging at different temperatures.

materials, higher self-discharge rates were obtained in the former at all temperatures, including the example temperatures of 60 and 75 °C. Indeed $LiMn_2O_4$ lost 100% of its initial capacity after only ~8 days of storage at 75 °C, whereas $LiCoO_2$ still retained ~40% capacity in the same conditions. This confirms the higher thermal stability of $LiCoO_2$ as compared to $LiMn_2O_4$.

4.2. Open-circuit voltage

The $e(t, T)$ curves during aging are traced in Fig. 3. The curves show two distinct voltage ranges: a '4 V' area with two slopped plateaus and, a '3 V' area with a flat plateau at 2.90–2.93 V. Between the '4 V' and the '3 V' segments, an intermediate area in the 3.6–2.90 V range is present. Except for the intermediate area, the '4 V' and '3 V' areas have the typical shape of low rate discharge curves in manganese spinel cathodes [39,40]. In fact, we have plotted in Fig. 4 the OCV versus composition 'x' curve obtained by GITT at the ambient temperature. It shows the '4 V' and '3 V' voltage plateaus, but does not show any intermediate area as the OCV sharply dropped between the two areas at composition close to $Li_1Mn_2O_4$.

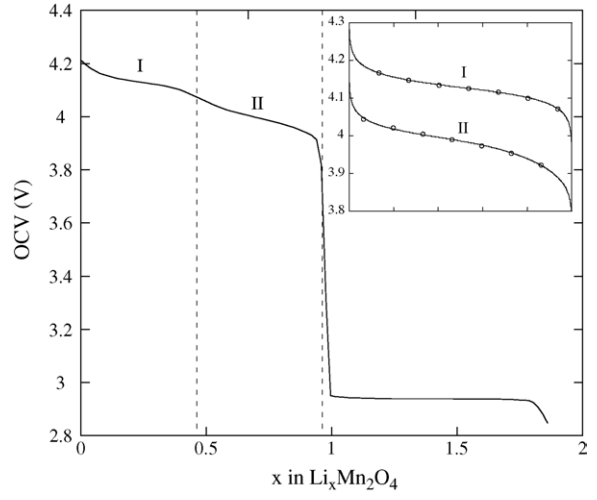

Fig. 4. The OCV vs. x curve of the Li/$Li_xMn_2O_4$ half cell at the ambient temperature obtained by GITT.

The $e(x)$ curve in Fig. 4 corresponds to the equilibrium state reached for a known amount 'x' of intercalated lithium in the spinel structure according to Eq. (2). The similarity in curves profile between $e(t, T)$ curves in Fig. 3 and the $e(x)$ curve in Fig. 4 strongly suggests that the mechanism governing the self-discharge is identical to that in the GITT curve, namely the lithium intercalation into λ-MnO_2. Such an intercalation corresponds to a chemical reduction of λ-MnO_2 and therefore it requires a source of electrons. Electrons are available from the electrolyte, as was suggested in the literature regarding $LiMn_2O_4$ [7–9] and $LiCoO_2$ [38]. The electrolyte oxidation may concern either PC, ClO_4^- or both. The latter can indeed form radical $ClO_4^\bullet$ as the result of a one-electron loss.

Accordingly a possible mechanism of self-discharge can be schematized as:

$$xE \leftrightarrow xE^+ + xe^- \tag{8}$$

$$Li_\varepsilon Mn_2O_4 + xLi^+ + xe^- \leftrightarrow Li_{\varepsilon+x}Mn_2O_4, \tag{2}$$

where E and E^+ design the electrolyte (PC and/or ClO_4^-) in the normal and oxidized forms, respectively.

In Fig. 5 we plotted side-by-side the $e(t, 75\,°C)$ and $e(x)$ curves in the '4 V' plateaus. The initial slope is steeper in the $e(t, 75\,°C)$ curve than in the $e(x)$ one, indicating a high self-discharge rate at the early steps of the thermal aging. The sloping voltage profile of the two '4 V' plateaus suggests single-phase rather than two-phase behavior.

The following empirical equations fit the $e(t, T)$ curves well:

- High '4 V' plateau:

$$e_1(t) = e_1^0 + k_1\, e^{-\lambda_1 t} + \alpha_1 \frac{RT}{F}\, \log \frac{1 - \mu_1\sqrt{t}}{\mu_1\sqrt{t}} \tag{9}$$

- Low '4 V' plateau:

$$e_2(t) = e_2^0 + \alpha_2 \frac{RT}{F}\, \log \frac{1 - \mu_2\sqrt{t}}{a + \mu_2\sqrt{t}} \tag{10}$$

The fitted curves for each plateau are shown in Fig. 6a and b, respectively, and the fitting parameters are displayed in Table 1.

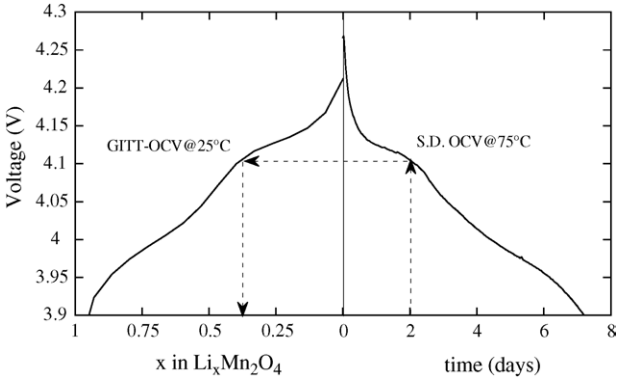

Fig. 5. OCV curves used to determine the electrode composition during aging.

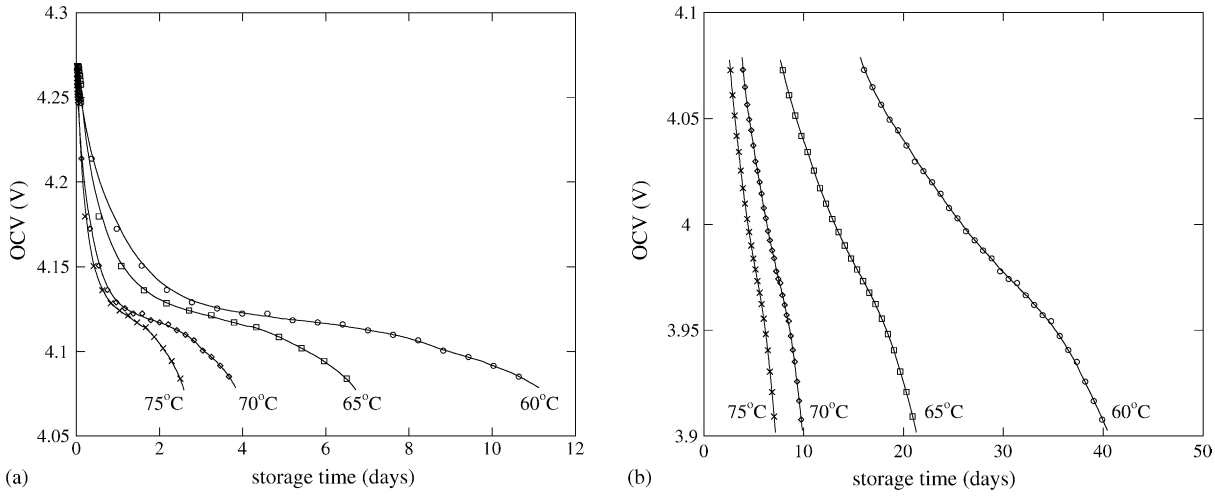

Fig. 6. Fits of the high 4 V (a) and low 4 V (b) plateaus during aging as given in Eqs. (9) and (10), respectively.

Table 1
Temperature dependence of the curve fitting parameters of Eqs. (9) and (10)

	T (°C)			
	60	65	70	75
e_1^0 (V)	4.126	4.131	4.127	4.131
k_1 (V)	0.107	0.121	0.105	0.121
λ_1 (day$^{-1/2}$)	1.152	2.053	3.480	5.338
α_1	0.413	0.470	0.428	0.457
μ_1 (day$^{-1/2}$)	0.296	0.379	0.502	0.611
e_2^0 (V)	4.002	4.000	4.002	4.000
α_2	1.557	1.544	1.559	1.543
μ_2 (day$^{-1/2}$)	0.150	0.206	0.303	0.355
a	−0.523	−0.502	−0.522	−0.503

Some parameters in Eqs. (9) and (10) such , e_1^0, e_2^0, k_1, α_1, α_2 and 'a' are temperature independent. The other parameters such as λ_1, μ_1 and μ_2 however, are thermally activated and follow the Arrhenius law. Their corresponding activation energies are given in Table 2.

The quick decay in the OCV curve at the beginning of self-discharge is largely accounted for the exponential term in Eq. (9). The latter might be governed by a first order kinetics law typical of a monoatomic reaction as might be expected from the electrolyte oxidation of Eq. (8). The $\sqrt{t}$ dependence in the logarithmic term of Eqs. (9) and (10) suggests a diffusion limited kinetics for longer aging times. Eq. (10) however, has no exponential term and the kinetics seems to be governed mainly by the lithium diffusion.

The $e(x)$ curve obtained by GITT in Fig. 4 was fitted with the following equations for the high ($i = 1$) and low ($i = 2$) '4 V' plateaus, respectively:

$$e_i(x) = E_i^0 + \beta_i \frac{RT}{F} \log \frac{1-x}{x} + \gamma_i x^{3/2} + \varphi_i x^4 \qquad (11)$$

The fitting parameters are given in Table 3. It shows remarkably high linear correlation coefficients $R^2 = 99.7\%$ of the fits on both '4 V' plateaus. The good fit is highlighted in the insert of Fig. 4 with the high and low plateaus areas marked I and II, respectively. Note the similar values of e_i^0 and E_i^0 ($i = 1, 2$) in Eqs. (9)–(11), respectively. The β_1 and β_2 values in Eq. (11) are close to unity, which shows the ion dominated interaction rather than the electronic one in $Li_xMn_2O_4$.

Dealing with the $(\gamma_i x^{3/2} + \varphi_i x^4)$ portion of Eq. (11), one should consider the cohesive energy in the $Li_xMn_2O_4$ ionic crystal with its general expression [41]:

$$u(r) = -\frac{\alpha e^2}{r} + \frac{C}{r^m}, \qquad (12)$$

where r is the ion–ion pair distance. The first term $-\frac{\alpha e^2}{r}$ is the electrostatic interaction and the second term $\frac{C}{r^m}$ comes from other forms of interaction such as dipole interactions. Since the average ion–ion distance r is proportional to $\frac{1}{\sqrt{x}}$ in a host structure with limited number of intercalation sites, the energy necessary to increment the amounts of lithium is given by:

$$dW(x) = \left(-\frac{\alpha e^2}{r} + \frac{C}{r^m}\right) dx = (\alpha' x^{1/2} + C' x^{m/2})\, dx \qquad (13)$$

Table 2
Activation energy of the curve fitting parameters in Eqs. (9) and (10) and of the self-discharge current peak intensity in three voltage domains areas

E_a (kJ mole^{-1})	High slope area	High '4 V' plateau	Intermediary area	Low '4 V' plateau
OCV $e(t, T)$	(λ_1) 98.6	(μ_1) 47.3	–	(μ_2) 57.4
Current peak	–	46.2	44.4	58.4

Table 3
Fitting parameters of the $e(x)$ curve at ambient temperature as in Eq. (11)

	High '4 V' plateau ($i = 1$)	Low '4V' plateau ($i = 2$)
E_i^0 (V)	4.119	3.982
β_i	0.97	0.95
γ_i	2.9×10^{-2}	2.3×10^{-2}
φ_i	-7.0×10^{-3}	-6.2×10^{-2}
R^2	0.999	0.997

Thus, the change in the cohesive energy between compositions 0 and x is expressed by:

$$W(x) = \int_0^x (\alpha' u^{1/2} + C' u^{m/2})\,\mathrm{d}u = Kx^{3/2} + Lx^{1+m/2}, \quad (14)$$

and the associated electric potential is:

$$e(W) = -\frac{W(x)}{F} = \gamma x^{3/2} + \varphi x^{1+m/2} \quad (15)$$

In Eq. (11), the best fit was found with $1 + m/2 = 4$, which corresponds to $m = 6$. Therefore, the second term in Eq. (12) is $\frac{C}{r^6}$ characteristic of fluctuating dipole interactions.

4.3. The self-discharge current

Fig. 5 shows the principle of x versus t correspondence using the OCV curves. In fact $e(t, T)$ and $e(x)$ are not measured at the same temperature. Therefore, the x versus t correspondence should be corrected by the entropy term as suggested in Eq. (5). However, using the $\Delta S(x)$ data found in the literature [42] did not significantly affect the 'x' values obtained from the OCV curves and the $\Delta S(x)$ correction was neglected here.

The resulting $x(t, T)$ curves are shown in Fig. 7. The curves do not vary linearly, which indicates a voltage dependant self-discharge current. The 100% self-discharge was reached in 8 days at 75 °C, and in 42 days at 60 °C. Using Eq. (3), we determined the time dependence of the self-discharge current at each temperature. The $i(e)$ curves are displayed in Fig. 8 with displays double x- and y-axes entries. The left y-axis uses the '$\sqrt{i}$' scale representation to magnify the weaker current intensities and the right entry uses the C/n rate scale for the self-discharge current. The top x-axis gives the composition corresponding to OCV 'e'.

The $i(e)$ curves show current peaks similar to those usually obtained by linear voltammetry. Current peaks appeared at 4.16, 4.08 and 3.99 V, respectively, and these voltages are basically temperature independent. Their intensity however, strongly depends on temperature and follows the Arrhenius law. The corresponding activation energy values are given in Table 2 together with those obtained from the $e(t, T)$ curves as discussed above.

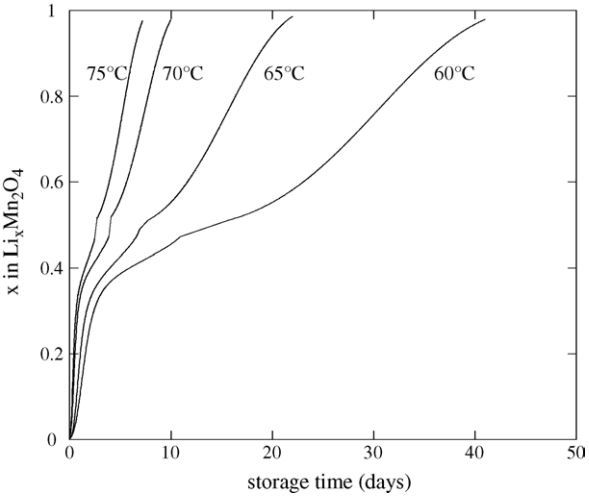

Fig. 7. The composition vs. time curves during thermal aging.

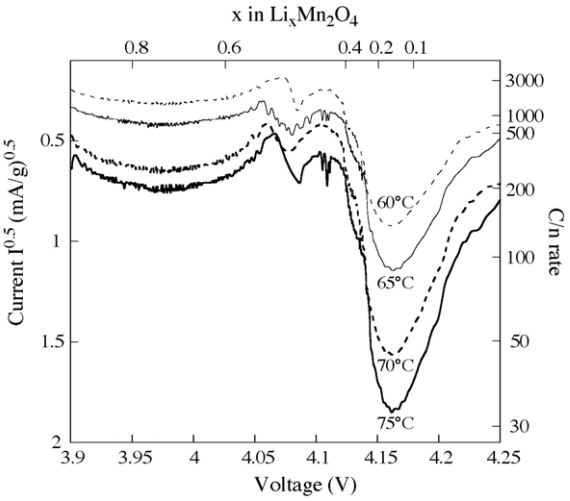

Fig. 8. Voltage and composition dependence of self-discharge current in a voltammetry-like representation (note the current is given the $\sqrt{i}$ scale on the left hand y-axis).

It is of interest to note that the values of activation energy obtained for the high and low '4 V' plateaus have similar values when determined from the $e(t, T)$ and $i(e)$ curves. Since in both cases the governing mechanism involves the lithium diffusion, we assume that these activation energies are those of the corresponding diffusion coefficients in the high and low '4 V' plateaus.

The other noteworthy result is that the self-discharge current varies significantly with the cell voltage and goes through peaks at well defined voltages. These voltages fall close to the inflexion points of the $e(x)$ curve. There are two types of inflexion points: the ones in the middle of each plateau which correspond approximately to half filling of the available lithium sites and the one at about 4.08 V between the two '4 V' plateaus, which is the onset of a phase transition. These results emphasize the correlation between the thermodynamics (sites filling, phase transition) and the kinetics (currents peaks) of the $LiMn_2O_4$ intercalation electrode.

The occurrence of irrecoverable capacity loss suggests some other mechanisms than lithium re-intercalation might be involved in the self-discharge. It is our argument that the irrecoverable capacity loss takes place mainly in the '3 V' plateau, where the cubic to the tetragonal phase transition occurs [12]. Such a transition is known to be irreversible in nature as it involves important cations rearrangement and a strong lattice distortion due to the Jahn–Teller effect. These structure changes are believed to be behind the observed capacity loss when the battery is cycled in the '3 V' even at the ambient temperature. Moreover, the manganese dissolution takes place at the '3 V' plateau as result of the Mn disproportionation [43], which could be another source of self-discharge.

5. Conclusion

We used the OCV curves obtained during the thermal aging of $Li/LiClO_4$ 1 M in $PC/LiMn_2O_4$ half-cells, and those obtained by GITT, to determine the self-discharge current and its voltage

dependence for the first time. Current peaks were found in the corresponding voltammograms, whose positions are temperature independent. The capacity loss is composed of two terms; a recoverable (reversible) loss associated with the lithium re-intercalation and a non recoverable (irreversible) loss, which we attributed to the spinel to tetragonal phase ($Li_2Mn_2O_4$) transition in the '3 V' plateau.

We found that our fits using empirical kinetics equations were in good agreement with the $e(t, T)$ and $e(x)$ OCV curves. This allowed the activation energy of each process to be determined. A correlation between the current peaks and the $e(t, T)$ curves was clearly established.

A crystal structure study is underway to support the lithium re-intercalation mechanism and the phase transitions in the 4 and 3 V areas.

Acknowledgement

Support for this project has been provided by DOE through Basic Energy Sciences Grant DE-FG03-00ER15035.

References

[1] D. Linden, Handbook of Batteries, second ed., McGrawHill, New York, 1995.
[2] Y. Nishi, in: M. Wakihara, O. Yamamoto (Eds.), Lithium Ion Batteries, Fundamental and Performances, Wiley-VCH, New York, 1998, p. 181.
[3] M.M. Thackeray, W.I.F. David, P.G. Bruce, J.B. Goodenough, Mater. Res. Bull. 8 (1983) 461.
[4] G. Pistoia, G. Wang, Solid State Ionics 66 (1993) 135.
[5] G. Amatucci, J.M. Tarascon, J. Electrochem. Soc. 149 (2002) K31.
[6] M. Broussely, S. Herreyre, P. Biensan, P. Kasztejna, K. Nechev, R.J. Staviewicz, J. Power Sources 97–98 (2001) 13.
[7] D. Guyomard, J.M. Tarascon, Solid State Ionics 69 (1994) 222.
[8] G. Pistoia, A. Antonini, R. Rosati, D. Zane, Electrochim. Acta 41 (1996) 2683.
[9] Y.Y. Xia, M. Yoshio, J. Power Sources 66 (1997) 129.
[10] T. Inoue, M. Sano, J. Electrochem. Soc. 145 (1998) 3704.
[11] A. Blyr, C. Sigala, G. Amatucci, D. Guyomard, Y. Chabre, J.M. Tarascon, J. Electrochem. Soc. 145 (1998) 194.
[12] J. Cho, M.M. Thackeray, J. Electrochem. Soc. 146 (1999) 3577.
[13] H. Huang, C.A. Vincent, P.G. Bruce, J. Electrochem. Soc. 146 (1999) 481.
[14] K. Nishimura, T. Douzono, M. Kasai, H. Andou, Y. Muranaka, Y. Kozono, J. Power Sources 81 (1999) 420.
[15] S.H. Kang, J.B. Goodenough, J. Electrochem. Soc. 147 (2000) 3621.
[16] E. Wang, D. Ofer, W. Bowden, N. Iltchev, R. Moses, K. Brandt, J. Electrochem. Soc. 147 (2000) 4023.
[17] D. Song, H. Ikuda, M. Wakihara, Electrochemistry 68 (2000) 460.
[18] T. Uchiyama, M. Nishizawa, T. Itoh, I. Uchida, J. Electrochem. Soc. 147 (2000) 2057.
[19] G.G. Amatucci, N. Pereira, T. Zheng, J.M. Tarascon, J. Electrochem. Soc. 148 (2001) A171.
[20] Y. Matsuo, R. Kostecki, F. McLarnon, J. Electrochem. Soc. 148 (2001) A687.
[21] G. Li, Y. Iijima, Y. Kudo, H. Azuma, Solid State Ionics 146 (2002) 55.
[22] H. Yamane, M. Saitoh, M. Sano, M. Fujita, M. Sakata, M. Takada, E. Nishibori, N. Tanaka, J. Electrochem. Soc. 149 (2002) A1514.
[23] Y.B. Chen, Q.G. Liu, J. Univ. Sci. Technol. Beijing 9 (2002) 197.
[24] J.S. Gnanaraj, V.G. Pol, A. Gedanken, D. Aurbach, Electrochem. Comm. 5 (2003) 940.
[25] M. Lanz, C. Kormann, P. Novak, J. Solid State Electrochem. 7 (2003) 658.
[26] M. Saitoh, M. Sano, M. Fujita, M. Sakata, M. Takata, E. Nishibori, J. Electrochem. Soc. 151 (2004) A17.
[27] Y. Shin, A. Manthiram, J. Electrochem. Soc. 151 (2004) A204.
[28] C.H. Lu, S.W. Lin, J. Mater. Res. 17 (2002) 1476.
[29] Y. Nishiwaki, Y. Terada, I. Nakai, Electrochemistry 71 (2003) 163.
[30] D. Aurbach, M.D. Levy, K. Gamulski, B. Markovsky, G. Salitra, E. Levi, U. Heider, L. Heider, R. Oesten, J. Power Sources 81 (1999) 47.
[31] M. Yoshio, Y.Y. Xia, T. Sakai, Electrochemistry 69 (2001) 516.
[32] M.M. Thackeray, Y. Shao-Horn, A.J. Kahaian, K.D. Kepler, E. Skinner, J.T. Vaughey, S.A. Hackney, Electrochem, Solid State Lett. 1 (1998) 7.
[33] Y.-K. Sun, C.S. Yoon, C.K. Kim, S.G. Youn, Y.-S. Lee, M. Yoshio, L.-H. Oh, J. Mater. Chem. 11 (2001) 2519.
[34] K.Y. Chung, W.S. Yoon, K.B. Kim, X.Q. Yang, S.M. Oh, J. Electrochem. Soc. 151 (2004) A484.
[35] S.S. Zhang, K. Xu, T.R. Jow, J. Electrochem. Soc. 149 (2002) A1521.
[36] M.M. Thackeray, A. de Kock, M.H. Rossouw, D.C. Liles, R. Bitthn, D. Hoge, J. Electrochem. Soc. 139 (1992) 364.
[37] C.J. Wen, B.A. Boukamp, R.A. Huggins, W. Weppner, J. Electrochem. Soc. 126 (1979) 2258.
[38] Y. Ozawa, R. Yazami, B. Fultz, J. Power Sources 119–121 (2003) 918.
[39] T. Ohzuku, M. Kitagawa, T. Hirai, J. Electrochem. Soc. 137 (1990) 769.
[40] M.M. Thackeray, J. Electrochem. Soc. 142 (1995) 2558.
[41] N.W. Ashcroft, N.D. Mermin, Solid State Physics, Rinehart and Wilson, Holt, 1976 (Chapter 20).
[42] K.E. Thomas, C. Bogatu, J. Newman, J. Electrochem. Soc. 148 (2001) A570.
[43] J.C. Hunter, J. Solid State Chem. 39 (1981) 142.